

Ternary Singular Value Decomposition as a Better Parameterized Form in Linear Mapping

Boyu Chen **Hanxuan Chen** **Jiao He**
 chenboyu17@huawei.com chenhanxuan@hisilicon.com hejiao4@huawei.com
Fengyu Sun **Shangling Jui**
 sunfengyu@huawei.com jui.shangling@huawei.com

Abstract

We present a simple yet novel parameterized form of linear mapping to achieve remarkable network compression performance: a pseudo SVD called Ternary SVD (TSVD). Unlike vanilla SVD, TSVD limits the U and V matrices in SVD to ternary matrices form in $\{\pm 1, 0\}$. This means that instead of using the expensive multiplication instructions, TSVD only requires addition instructions when computing $U(\cdot)$ and $V(\cdot)$. We provide direct and training transition algorithms for TSVD like Post Training Quantization and Quantization Aware Training respectively. Additionally, we analyze the convergence of the direct transition algorithms in theory. In experiments, we demonstrate that TSVD can achieve state-of-the-art network compression performance in various types of networks and tasks, including current baseline models such as ConvNext, Swim, BERT, and large language model like OPT.

1 Introduction

Linear mapping, which includes fully connected layers and convolution layers, is a crucial component of modern neural networks in most cases. It accounts for virtually all parameter counts and FLOPS of the entire network and is always the primary target in network compression.

The current weight compression method for a linear mapping can be broadly classified into three principles (Neill 2020): quantization, low rank decomposition, and pruning. Many current works, including (Zafir et al. 2021; Li et al. 2021; Guo et al. 2022; Jaderberg, Vedaldi, and Zisserman 2014; Frantar and Alistarh 2023; Frantar et al. 2022), focus solely on improving the fine-tuning and calibration procedures based on these principles. However, the representation accuracy of these principles limits the upper limit of their effectiveness, particularly in the case of super low-bit quantization.

In recent years, a new principle has emerged: using cheap addition instructions instead of the expensive multiplication instructions for acceleration. This approach has been explored in various works, including (Chen et al. 2020; You et al. 2020; Courbariaux, Bengio, and David 2015). However, all of these approaches require building a specific model architecture and training from scratch, which makes them impractical for large language models.

In this paper, based on this new principle, we propose Ternary SVD (TSVD) as an improved parameterized form of

linear mapping, building upon the ideas of SVD and AdderNet(Chen et al. 2020). TSVD limits the U and V matrices of SVD into two Ternary matrices in $\{\pm 1, 0\}$. Unlike vanilla SVD, the rank of TSVD is typically not small. Based on the results of fitting random matrices in Figure 1a, it is evident that our TSVD approach, which is based on the new principle, outperforms quantization, low rank decomposition and pruning. In short, our contributions in this paper are as follows:

- We introduce TSVD as a new parameterized form of linear mapping, which is significantly accelerated by replacing multiplication instructions with sparsity additions. To the best of our knowledge, TSVD is the first data-independent ternary PTQ method that is suitable for a wide range of network scales and tasks while maintaining high accuracy.
- We analyze the convergence of the direct transition algorithm in theory. Also, we introduce a simple yet novel way of STE in TSVD QAT algorithms.
- In experiments, we demonstrate that TSVD can achieve state-of-the-art network compression performance in various types of networks and tasks, including current baseline models such as ConvNext, Swim, BERT, and large language model like OPT.

2 Preliminary

2.1 Truncated SVD in Network Compression

We will begin by examining the compression of vanilla SVD in a fully connected layer. Consider a scenario where there is a single input sample on the fully connected layer without any bias. The equation is as follows:

$$y = Wx \quad (1)$$

where W is a parameter matrix with shape $[M, N]$, y is the output vector with shape $[M, 1]$, and x is an input vector with shape $[N, 1]$. Vanilla SVD decomposes W into three parameter tensors U , S , and V by solving the following optimization problem:

$$U, S, V = \arg \min_{U, S, V} \|U \text{diag}(S)V - W\|_F \quad (2)$$

where U is a column orthogonal matrix of shape $[M, K]$, V is a row orthogonal matrix of shape $[K, N]$, and S is a singu-

lar vector of shape $[K]$. If $U \text{diag}(S)V$ can closely approximate W , then eq 1 can be computed using the following formula:

$$y = Wx \simeq U(\text{diag}(S)(Vx))$$

For vanilla SVD, a low rank K is required for network compression. However, in practice, achieving a good approximation of W under such low K conditions can be challenging. Previous SVD methods for network compression have often faced difficulties in balancing the tradeoff between approximation and acceleration. The critical rank K (denoted as \bar{K}) that balances FLOPS with and without vanilla SVD is simply:

$$\bar{K} = \frac{MN}{M+N}$$

2.2 Hardware Cost of Basic Instruction

For hardware implementation, the addition instruction is often much cheaper than multiplication. Previous works have proven effective by making the most use of feature, including (Courbariaux, Bengio, and David 2015; Lavin and Gray 2016; Chen et al. 2020; You et al. 2020). However, accurately comparing their costs depends on the specific hardware and which cost we are concerned with. Theoretical estimates suggest that d -bit addition costs $\mathcal{O}(d)$ and multiplication costs $\mathcal{O}(d^2)$, which aligns with the energy data from (You et al. 2020; Zhang, Zhang, and Lew 2022). However, estimating latency cost in such way is usually too ideal, although the order of magnitude is still correct. In this paper, since there always exist a sign bit in d -bit presentation and there is $d-2$ addition in the long multiplication algorithm of $d-1$ bit unsigned integer, to avoid overcomplicating the problem, we simply assume that

$$1 \times \text{Mul} = (d-2) \times \text{Add}$$

for principle elucidation and experiment intuitive understanding, while also providing actual multiplication and addition counts in our experiments for custom assessment.

3 Ternary SVD

Ternary SVD, regardless of how to solve it, can also be defined as the optimization problem of (2), with the additional constraint that U and V are both Ternary matrices in $\{\pm 1, 0\}$. This allows for the use of addition instructions instead of multiplication instructions in computing $U(\cdot)$ and $V(\cdot)$, resulting in faster computation. Compared to vanilla SVD, TSVD has a more relaxed constraint on the rank K for acceleration. The critical rank \bar{K} of Ternary SVD is given by

$$\bar{K} = \frac{(d-1)MN}{d+r(M+N)-2} \quad (3)$$

where d is the bit-width and r is the sparsity rate (non-zero rate) of U and V (a detailed derivation can be found in section S1.1). As shown in figure 1a, it is evident that TSVD outperforms previous compression principles in terms of the tradeoff between compression rate and approximation error in a simple random matrix test with Laplace distribution.

3.1 Direct Transition Algorithm to TSVD form

We have developed a simple greedy algorithm to perform this transformation, which is based on the main belief that *the largest TSVD component of W should be close to the simply ternarization of the largest SVD component* (illustrated in figure 1b). We begin by initializing the residual $R = W$, and then proceed with the following iterations until the exit condition is met.

1. Do SVD of R to get its top- q component of U, V , noted as U', V' .
2. Ternarize U', V' as a set of row vector and column vector separately, and append them into existing U, V .
3. Calculate $S = \arg \min_S \|W - U \text{diag}(S)V\|_F$.
4. Calculate $R = W - U \text{diag}(S)V$.

The ternarization policy in step 2 can be summarized as follows: *Given a unit vector x , the goal is to find the most sparse ternary vector x_T^* that satisfies the constraint that the angle between x and ternary vector x_T is less than or equal to a certain threshold θ* . It is important to note that x_T^* has a specific structure (proved in section S1.2):

$$\begin{aligned} x_T^*[i] &= 0 \text{ or } \text{sign}(x[i]), \forall i \\ \arg \text{nonzero}(x_T^*) &= \arg \text{top.k}(\text{abs}(x), q), \exists q \end{aligned} \quad (4)$$

Therefore, instead of traversing all possible $3^{\#(x)}$ Ternary vectors, we only need to traverse $\#(x)$ ternary vectors to find the optimal ($\#(x)$ denote the dimensions of x). The complete ternarization algorithm can be viewed in algorithm 1.

Algorithm 1: Ternarization algorithm $T(\cdot)$ (in numpy style), return the most sparsity ternary vector in the set in which angle to x is less or equal to θ .

Input: x, θ // x is vector, θ is angle threshold.

- 1 $o_x \leftarrow \text{np.sort}(\text{np.abs}(x))[:, -1]$
- 2 $s_x \leftarrow \text{np.cumsum}(o_x)$
- 3 $n_x \leftarrow \text{np.sqrt}(\text{np.arange}(1, x.\text{size}+1))$
- 4 $c_x \leftarrow s_x / n_x$
- 5 $i_x \leftarrow \text{np.argmax}(c_x \geq \cos(\theta))$
- 6 **if** $c_x[i_x] < \cos(\theta)$ **then**
- 7 \perp raise error // T_x does not exist.
- 8 $t_x \leftarrow \text{np.where}(x \geq 0, 1, -1)$
- 9 $t_x \leftarrow \text{np.where}(\text{np.abs}(x) \leq o_x[i_x], 0, t_x)$

Output: t_x as the ternarization of x .

To establish the existence of x_T^* , we rely on the following theory (for a more detailed explanation, please refer to section S1.3):

Theorem 1. *Considering an N -dimensional unit vector $a \in \mathbb{S}^{N-1}$, there must exist a ternary vector $t \in \{\pm 1, 0\}^N$ to ensure that their angle θ' satisfies:*

$$\cos(\theta') = \frac{\langle a, t \rangle}{\sqrt{\|t\|_0}} \geq \frac{1}{\underbrace{\sqrt{\sum_{k=1}^N (\sqrt{k} - \sqrt{k-1})^2}}_{\gamma_N}}$$

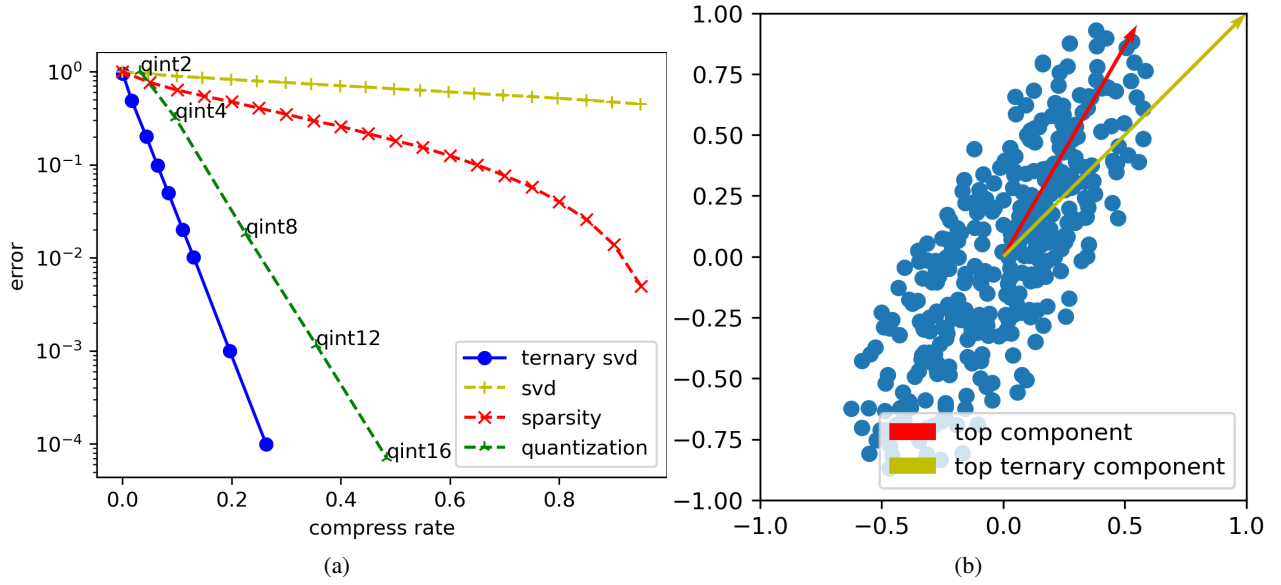


Figure 1: (a): For various network weight compression methods, tradeoff between compression rate, and relative operator norm error on a $[512, 256]$ float32 random matrix with Laplace distribution. Our method is represented by the blue line. For more detail, see section S2.1. (b): Illustration of the main belief of our greedy algorithm 2 in 2 dimension. We can view the SVD decomposition as a PCA process to the column or row vector of W . The goal of TSVD definition is to find the top ternary component (indicated by the yellow arrow). To achieve this, we first identify the top component (indicated by the red arrow) and then convert it into its closest ternarization vector.

remark 1. It can be inferred that the threshold γ_N decreases at a rate of $\frac{1}{\sqrt{\log(N)}}$. Although it still approaches zero while N approaches infinity, it decreases very slowly and can reach a minimum value of $\gamma_N \geq \cos(\frac{\pi}{4})$ when $N \leq 55$. Moreover, in practice, we need not worry about the existence of x_T^* even if we set the threshold $\theta \geq \cos(\frac{\pi}{4})$ when $N > 55$ (see section 3.2). This may be related to the specific parameter distribution and requires further exploration.

For step 3, it is an obvious least squares problem and the optimal solution for S , denoted as S^* , can be obtained by the following equation (for more details, see section S1.4):

$$S^* = [(U^T U) \odot (V V^T)]^\dagger \text{diag}(U^T W V^T) \quad (5)$$

where \odot denotes the Hadamard product and $(\cdot)^\dagger$ denotes the Moore-Penrose pseudo-inverse. The entire direct transition algorithm to TSVD form is shown in algorithm 2.

For convergence in theory, we propose theorem 2 (proved in section S1.5):

Theorem 2. Considering a single iteration in algorithm 2, and assuming that $\theta > \frac{\pi}{4}$ and $q = 1$, we can define \bar{S} as the argument that minimizes $\|R_i - T_u \text{diag}(\bar{S}) T_v\|_F$. In this case, the singular vector of R_i (sorted in descending order) is denoted by σ_i , and follows that:

$$\begin{aligned} \|R_i - T_u \text{diag}(\bar{S}) T_v\|_F^2 &\leq \sin^2(2\theta) (\sigma_i[0])^2 + \|\sigma_i[1:] \|_2^2 \\ &\leq \left(1 - \frac{\cos^2(2\theta)}{\min(M, N)}\right) \|R_i\|_F^2 \end{aligned}$$

Corollary 1. In fact, compared to the default algorithm 2, theorem 2 proves convergence on a weaker update policy

of s_i by fixing the exist dimensions and just optimizing on the new dimension on the tail. More specifically, when $\theta > \frac{\pi}{4}$, $q = 1$, such weaker update policy is:

$$\bar{S} \leftarrow \arg \min_s \|R_i - T_u \text{diag}(S) T_v\|_F$$

$$S_{i+1} \leftarrow \text{np.concatenate}([S_i, \bar{S}], \text{axis} = 0)$$

This is because under this policy, it must have

$$R_{i+1} = R_i - T_u \text{diag}(\bar{S}) T_v$$

Hence, we can infer that algorithm 2 must converge at least linearly at a rate of $\sqrt{1 - \frac{\cos^2(2\theta)}{\min(M, N)}}$ when $\theta > \frac{\pi}{4}$, $q = 1$.

remark 2. We still employ a stronger update policy in algorithm 2 for S_i to prevent the duplication vectors in U_i and V_i . Additionally, we have relaxed the constraint for $q > 1$ in consideration acceleration.

3.2 Optimal θ in Practice

To determine the optimal value of θ in practice, we analyzed the relationship among the relative operator norm error, compress rate, and the θ threshold. Our testing was conducted on a $[512, 256]$ float32 random matrix with Laplace distribution, and the results are presented in figure 2a. We found that the optimal value of θ is achieved when $\theta = 0.576(33^\circ)$ for any tolerance error configuration. Under such θ the sparsity rate r is about 0.29. These configuration and sparsity rate are stable for various tasks and bit-widths. In this paper, unless otherwise specified, all experiments will be conducted using this configuration and will not additionally report sparsity rate by default.

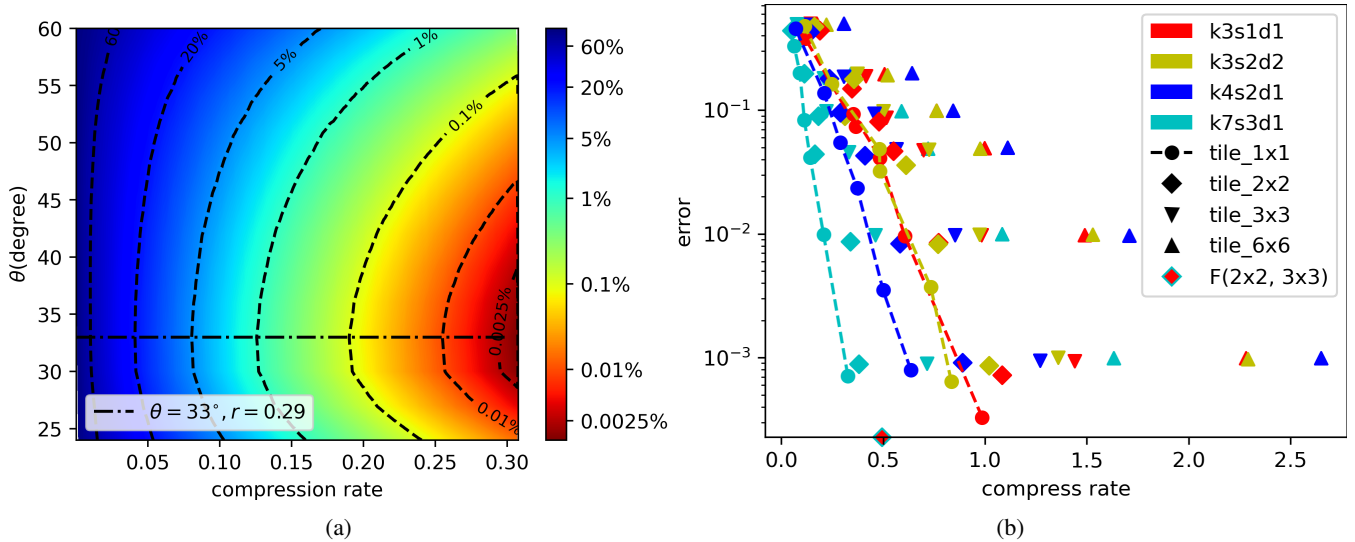


Figure 2: (a): The optimal threshold θ selection on a randomly generated float32 matrix with shape $[512, 256]$ and Laplace distribution. The color in the graph represents the relative error of operator norm. We observed that to achieve the optimal compression rate, the optimal θ value is approximately 0.576 (equivalent to 33 degrees). At this threshold, the sparsity rate r is about 0.29.(b): Tradeoff between compression rate, and relative operator norm error for various single-channel float32 convolutions with different tile unfoldings. Each convolution is represented by a different color, and each tile configuration is represented by a different marker shape. We also highlighted the Winograd $F(2 \times 2, 3 \times 3)$ in our figure. More experiment detail see section S2.2.

3.3 TSVD in Convolution Layer

For convolution, the most intuitive way to use TSVD is to unfold the kernel into a small tile as a cyclic matrix and process it as a normal linear map. For instance, we can use the Winograd symbol and consider a one-dimensional convolution of $F(2, 3)$, which can be unfolded as follows:

$$\begin{pmatrix} y_1 \\ y_2 \end{pmatrix} = \underbrace{\begin{pmatrix} w_1 & w_2 & w_3 & 0 \\ 0 & w_1 & w_2 & w_3 \end{pmatrix}}_{\mathcal{W}} \begin{pmatrix} x_1 \\ x_2 \\ x_3 \\ x_4 \end{pmatrix}$$

Then, we can perform TSVD on \mathcal{W} . In figure 2b, after testing various configurations of tile, stride, dilation, and kernel size, we found that when taking into account the sparsity of \mathcal{W} itself, it has:

- For each convolution configuration, all points lie on the top-right side of the curve for tile_1x1 in figure 2b, indicating that tile_1x1 is the optimal tile configuration for convolution TSVD.
- For tile_1x1, larger kernel size yields a better compression rate, suggesting that larger kernels are easier to compress.
- Convolution TSVD can achieve a 4% error when the compression rate is equivalent to that of $F(2 \times 2, 3 \times 3)$

Therefore, we can simplify the algorithm as the previous convolution low rank decomposition method does. According to the work of (Zhang et al. 2015; Jaderberg, Vedaldi, and Zisserman 2014), we both consider channel-wise and

spatial-wise decompositions, i.e. we reshape the kernel into one of the four shapes in eq (6) and select the optimal one of the compression rate as the result of TSVD in the convolution layer.

$$\begin{aligned} & [C_{out}, C_{in} \times K_1 \times K_2] \\ & [C_{out} \times K_1 \times K_2, C_{in}] \\ & [C_{out} \times K_1, C_{in} \times K_2] \\ & [C_{out} \times K_2, C_{in} \times K_1] \end{aligned} \quad (6)$$

After decomposition, $U(\cdot)$ and $V(\cdot)$ can be computed in convolution form, and $\text{diag}(s)(\cdot)$ can be calculated as a channel-wise multiplication operator. The kernel shape corresponding to the four shape matrices in eq (6) is:

$$\begin{aligned} \text{kernel}_U &= [1, 1], & \text{kernel}_V &= [K_1, K_2] \\ \text{kernel}_U &= [K_1, K_2], & \text{kernel}_V &= [1, 1] \\ \text{kernel}_U &= [K_1, 1], & \text{kernel}_V &= [1, K_2] \\ \text{kernel}_U &= [1, K_2], & \text{kernel}_V &= [K_1, 1] \end{aligned}$$

Connection with Winograd It can be inferred that the most commonly used Winograd convolution form, $F(2 \times 2, 3 \times 3)$, is actually *one of the special lossless cases of TSVD on a tile of size 2×2* . As shown in figure 2b, our algorithm with a tile size of 1×1 can achieve a better compression rate than Winograd $F(2 \times 2, 3 \times 3)$ when tolerance error is great or equal to 4%. Another advantage of decomposing on a tile size of 1×1 is that our algorithm can adapt to any configurations of stride, padding, and dilation. Even on depth-wise convolution with a large kernel, our algorithm can obtain a pretty good compression rate, giving us

Algorithm 2: Direct transition algorithm to TSVD form

Input: $W, \theta, q = 1, R_0 = W, U_0 = \emptyset, V_0 = \emptyset$
1 $i \leftarrow 0$
2 **while** not exit condition meet **do**
3 $u, -, v \leftarrow \text{np.linalg.svd}(R_i, \text{full_matrices}=\text{False})$
4 $T_u \leftarrow \text{vmap}(T(\cdot, \cdot), \text{in_axes}=(1, \text{None}), \text{out_axes}=1)(u[:, 0:q], \theta)$
5 $T_v \leftarrow \text{vmap}(T(\cdot, \cdot), \text{in_axes}=(0, \text{None}), \text{out_axes}=0)(v[0:q, :], \theta)$
// Ternarize the top- q column vector of u , and top- q row column vector of v . See algorithm 1.
6 $U_{i+1} \leftarrow \text{np.concatenate}([U_i, T_u], \text{axis}=1)$
7 $V_{i+1} \leftarrow \text{np.concatenate}([V_i, T_v], \text{axis}=0)$
8 $S_{i+1} \leftarrow [(U_{i+1}^\top U_{i+1}) \odot (V_{i+1} V_{i+1}^\top)]^\dagger \text{diag}(U_{i+1}^\top W V_{i+1}^\top)$
9 $R_{i+1} \leftarrow W - U_{i+1} \text{diag}(S_{i+1}) V_{i+1}$
10 $i \leftarrow i + 1$

Output: U_i, S_i, V_i , where $U_i \text{diag}(S_i) V_i \simeq W$

greater flexibility compared to fixed decomposition methods like Winograd.

3.4 Training TSVD in QAT style

For very low bit training, including BNN, the key essential of QAT training or finetuning is how to back-propagate through the quantized parts. To achieve this, we still use the Straight-Through Estimator (STE) for TSVD QAT training but in a novel way. *Instead of considering how to back-propagate to U, S and V , we view the entire TSVD result of W as a quantization form of W and apply STE to it.* Specifically, we perform this process during forwarding:

$$\begin{cases} U, S, V = \text{TSVD}(W) \\ \bar{W} = U \text{diag}(S) V \\ y \simeq \bar{W} x \end{cases}$$

and do such STE in back-propagation:

$$\frac{\partial \mathcal{L}}{\partial W} \simeq \frac{\partial \mathcal{L}}{\partial \bar{W}}$$

Hence, we need to redo the TSVD of W every time the optimizer updates the parameters. This task is computationally intensive, so we only hold the main row and column vectors of V and U corresponding to the top S values, and recompute their tail part. This approach is outlined in algorithm 3. For the convolution layer, the matrix type in eq 6 is only reselected when the main row and column vectors of V and U are empty.

4 Experiment

We test TSVD on various scales of neural networks and tasks, consistently setting $\theta = 0.576$ as demonstrated in section 3.2, setting a self-adaptive q to guarantee at least 20 iterations in algorithm 2. The only hyperparameter in our algorithm that requires tradeoff is the tolerance error. We follow

Algorithm 3: Recompute policy in TSVD QAT training.

Input: $W^{t+1}, U^t, V^t, \eta, \theta$
// η is the threshold of main-tail split.
1 $S \leftarrow [(U^{t\top} U^t) \odot (V^t V^{t\top})]^\dagger \text{diag}(U^{t\top} W^{t+1} V^{t\top})$
2 $R \leftarrow W - U^t \text{diag}(S) V^t$
3 $U', S', V' \leftarrow \text{TSVD}(R, \theta, \text{rank} = 1)$
// get the maximum TSVD singular of the residual.
4 $m \leftarrow S \sqrt{\text{diag}(U^{t\top} U^t) \text{diag}(V^t V^{t\top})} > \eta S' \|U'\| \|V'\|$
5 $U, V \leftarrow U^t[\dots, m], V^t[m, \dots]$
6 $S \leftarrow [(U^\top U) \odot (V V^\top)]^\dagger \text{diag}(U^\top W^{t+1} V^\top)$
7 $R \leftarrow W - U \text{diag}(S) V$
// recompute the residual after determine the main part.
8 $U^{t+1}, S^{t+1}, V^{t+1} \leftarrow \text{TSVD}(W^{t+1}, \theta, R_0 = R, U_0 = U, V_0 = V)$ // algorithm 2
Output: $U^{t+1}, S^{t+1}, V^{t+1}$

the method presented in table S2 for the translation of acceleration rate of all comparative items. Due to computational limitations, we only present the finetune results of the image task. All experiments are conducted on a single GPU node equipped with $8 \times$ Nvidia Tesla V100 32G GPUs, and the results are presented as the mean of three runs.

4.1 Experiment on ImageNet 1K

We test ConvNeXt-T (Liu et al. 2022), Swin-T (Liu et al. 2021) and ResNet-50 (He et al. 2016) on ImageNet 1K (Rusakovsky et al. 2015) dataset and showed in table 1. One should be highlight is that different to the previous compression method like (Chen et al. 2020) or (Li et al. 2021), our method has enough accuracy hence we transform *all linear and convolution layers in those networks, including the convolution layers in stem, fully connect layer in head, and all depth-wise convolution*. Note these three network architecture are quite different: ResNet50 is the classic baseline with 3×3 convolution, Swin-T is the compact visual transform architecture, and ConvNeXt-T is composed by 1×1 convolution with large channel and depth-wise convolution with large kernel. TSVD can achieve high acceleration rate with almost lossless accuracy drop on all three models. The final sparsity rate and rank K for each layer can be viewed in section S2.3

4.2 Experiment on BERT

We run experiment on our TSVD method using the BERT base model (Devlin et al. 2018) and the GLUE dataset (Wang et al. 2018). As in section 4.1, we applied TSVD to the last fully connected head layer, but not to the embedding layer, as it does not contain any FLOPS. The sequence length was fixed at 128, and for each downstream task in GLUE, we first fine-tuned the model as usual, then performed a direct TSVD transition at the end. The computa-

Table 1: TSVD tests on Imagenet 1k using various networks. The acceleration rate estimated by d bit-width is expressed as $\text{acc}(d)$, although every network was actually run under float32. $\times(B)$ denote the multiplication billion counts, $+(B)$ denote the addition billion counts, $\times + (B)$ denote the multiply-accumulate billion counts. F denote finetuning.

Model	Method	$\times(B)$	$+(B)$	$\text{acc}(d=32)$	$\text{acc}(d=8)$	params (M)	tern params (M)	top-1(%)
ConvNeXt-T	original	4.47	4.46	$\times 1$	$\times 1$	28.6	0	82.07
	1% tol TSVD	0.074	12.6	$\times 9.34$	$\times 2.40$	0.23	279.3	82.05
	7% tol TSVD (F)	0.046	6.12	$\times \mathbf{18.47}$	$\times \mathbf{4.89}$	0.15	129.78	82.04
Swin-T	original	4.50	4.50	$\times 1$	$\times 1$	28.3	0	80.40
	1% tol TSVD	0.21	12.3	$\times 7.50$	$\times 2.32$	0.29	261.8	80.37
	7% tol TSVD (F)	0.18	5.84	$\times \mathbf{12.41}$	$\times \mathbf{4.55}$	0.19	109.03	80.34
ResNet-50	original	4.10	4.10	$\times 1$	$\times 1$	25.6	0	75.85
	1% tol TSVD	0.060	10.83	$\times 10.06$	$\times 2.56$	0.21	242.5	75.81
	7% tol TSVD (F)	0.035	4.99	$\times \mathbf{21.04}$	$\times \mathbf{5.51}$	0.16	105.23	75.79
	AdderNet(Chen et al. 2020)	0.131	8.08	$\times 10.58$	$\times 3.24$	25.6	0	74.94
		$\times + (B)$		acc		params (M)		
	CC($C = 0.5$)(Li et al. 2021)	1.93		$\times 2.12$		13.2		75.59
LRPET($P = 0.62$)(Guo et al. 2022)	1.90		$\times 2.15$		12.89		75.91	

tion cost after TSVD for various downstream tasks was similar, so we only report the mean of multiplication, addition, and parameter count of these downstream tasks. Compared to the original BERT base, TSVD achieved an acceleration rate of $\times 8.75$ with almost no loss in accuracy, and $\times 13.45$ with only a slight loss in accuracy, which exceeds the current state-of-the-art method, such as prune OFA (Zafir et al. 2021).

4.3 Experiment on OPT

To evaluate our method on large language models, we conducted experiments on all linear layers of OPT-6.7B (Zhang et al. 2022) with a full sequence length of 2048, including the last `lm_head` layer. As shown in Table 3, our method achieved an acceleration rate of approximately $\times 4.64$ and produced the most lossless results on wikitext2 (Merity et al. 2016), ptb (Dinarelli and Grobol 2019), and c4 (Raffel et al. 2019). Our acceleration rate is better than the current state-of-the-art methods such as GPTQ (Frantar et al. 2022) and sparseGPT (Frantar and Alistarh 2023), while our method does not have an advantage in parameter storage. The acceleration rate calculation method follows the approach outlined in table S2.

5 Conclusion and Discussion

In this paper, we introduce Ternary SVD as an improved parameterized form of linear mapping. By combining low-bit quantization and SVD, Ternary SVD effectively vanishes the number of multiple instructions in fully connected and convolution layers. We provide direct and training transition algorithms for Ternary SVD like Post Training Quantization and Quantization Aware Training respectively. Additionally, we analyze the convergence of the direct TSVD transition algorithms in theory. Our experiments demonstrate that Ternary SVD achieves state-of-the-art network compression performance across various networks and tasks, including current baseline models like ConvNext, Swim, BERT, and large language model like OPT.

However, there are still some bottlenecks that prevent the out-of-the-box usage of TSVD. The main issue is that al-

though the compute cost is theoretically $\mathcal{O}(d)$ for d -bit addition instructions and $\mathcal{O}(d^2)$ for d -bit multiplication instructions separately, as far as we know, the main vectorized computation platforms like CUDA or MKL do not optimize for it and still assign the same instruction cycle. Therefore, in practice, it is currently unavailable to achieve the wall-time advantage of TSVD as guaranteed by theory on the mainstream hardware platforms. This is also the reason why we only report the counts of addition and multiplication instructions and do not show the wall-time latency in our experiments.

Another issue is the sparsity acceleration problem. While sparsity is an attractive feature in TSVD, it is not friendly in vectorized computation and has been a study for many years in research. However, recent advancements in vectorized computation have proposed structured sparsity instructions, e.g. in (Mishra et al. 2021) the 2:4 sparse tensor core in Nvidia A100 GPU. One of our future works is to further constrain TSVD to satisfy the structure of these instructions.

For large language models, although our method achieves remarkable acceleration performance compared to other low-bit compression algorithms, it does not provide an advantage in terms of parameter storage. However, we are relatively optimistic about this issue because the ternary matrix U and V are quite sparse, and the current 2-bit presentation is overly redundant. Presenting in a more efficient way is another future work in our plan.

Additionally, we would like to discuss the connection between BNN and its potential evolution in the end of this paper.

5.1 Connection with BNN and What Next

In a sense, TSVD can also be seen as the weight component of the BNN PTQ transition. This is due to the fact that we can decompose U and V into their positive and negative parts:

$$\begin{cases} U = U_+ - U_- \\ V = V_+ - V_- \end{cases}$$

where U_+, U_-, V_+, V_- are binary matrices in $\{0, 1\}$. One important thing to highlight is that *such decomposition is not*

Table 2: BERT experiment on GLUE dataset. The acceleration rate estimated by d bit-width is expressed as $\text{acc}(d)$, although every network was actually run under float32. P / TP (M) represents the standard parameters and ternary parameters in millions. $\times / + (B)$ denote the multiplication and addition billion counts, $\times + (B)$ denote the multiply-accumulate billion counts.

Model	Method	$\times / + (B)$	$\text{acc}(d=32/4)$	P / TP (M)	CoLA	SST-2	MRPC	STS-B	QQP	MNLI	QNLI	RTE
					Matthews Corr	Accuracy	F1 / Accuracy	Pearson / Spearman	F1 / Accuracy	M / MM	Accuracy	Accuracy
BERT base	original	11.19 / 11.18	$\times 1 / 1$	109 / 0	59.33	92.78	89.19 / 84.55	87.52 / 87.23	87.50 / 90.81	83.79 / 84.27	90.61	64.26
	1% tol TSVD	0.34 / 29.40	$\times 8.75 / 1.47$	23 / 825	60.81	92.43	89.03 / 83.57	88.47 / 88.28	87.42 / 90.68	83.50 / 84.36	90.57	65.70
	5% tol TSVD	0.33 / 15.88	$\times 13.45 / 2.65$	23 / 440	60.65	91.05	89.78 / 85.04	87.57 / 87.40	86.71 / 89.51	83.11 / 82.75	89.36	61.01
			$\times + (B)$	params(M)								
	85% prune OFA (Zafir et al. 2021)		1.94	$\times 5.76$	109	41.51	90.48	87.25 / 82.60	82.86 / 83.13	84.44 / 88.53	78.89 / 79.53	88.01
90% prune OFA (Zafir et al. 2021)		1.40	$\times 7.99$	109	35.60	88.76	83.90 / 75.74	81.53 / 82.08	83.73 / 87.84	77.61 / 78.36	86.91	56.32

Table 3: Experiment on the language generation model OPT-6.7B with a sequence length of 2048, evaluating the acceleration rate when $d = 16$. The notation $\times (T)$ represents trillion multiplications counts, while $+(T)$ represents trillion additions counts. $\times + (T)$ denotes trillion multiply-accumulate operations counts with a specific weight and activation bit width. The indicator of datasets wikitext2, ptb and c4 is Perplexity (PPL).

Model	Method	$\times (T)$	$+(T)$	$\text{acc}(d=16)$	params (B)	tern params (B)	wikitext2	ptb	c4	
OPT 6.7b	original	14.72	14.72	$\times 1$	6.86	0	10.86	13.08	11.74	
	1% tol TSVD	1.11	31.98	$\times 4.64$	0.22	55.03	11.10	13.73	12.16	
	1.5% tol TSVD	1.11	27.66	$\times 5.11$	0.22	47.37	12.12	15.62	13.34	
	2% tol TSVD	1.11	24.64	$\times 5.49$	0.22	42.00	19.08	26.06	25.75	
			W16A16, $\times + (T)$	Wd'A16, $\times + (T)$	acc	params (B)	d'-bit params (B)			
	4-bit GPTQ	1.53	13.19	$\times 3.75$	0.43	6.41	11.39	13.77	12.14	
	3-bit GPTQ	1.53	13.19	$\times 4.66$	0.43	6.41	14.98	18.67	15.54	
	50% sparseGPT	8.13	0	$\times 1.81$	6.86	0	11.59	17.38	13.72	
	50% sparseGPT + 4 bit	1.53	6.59	$\times 5.16$	0.43	6.41	12.23	18.16	14.22	

only mathematically equivalent, but also equivalent in terms of FLOPS counts and parameter storage. The equivalence in parameter storage is due to that we only need 2 bits to store each element of a ternary matrix, and 1 bit of a binary matrix. The equivalence in FLOPS counts is due to that if there is a ± 1 element in U , there should be only one 1 in U_+ or U_- at the corresponding index.

Therefore, a natural and appealing idea is to further develop the BNN PTQ method by exploring how to binarize the feature map in the middle layer of networks. However, whether this can be achieved or not, such idea is not a proper question. This is because the computational cost of d -bit addition instruction is $\mathcal{O}(d)$, and the computation cost in network layers dominated by addition is always proportional to the total bits of the input feature map, regardless of the bit width in computation. Therefore, transitioning to a binary feature map is unhelpful if the total bits of the input feature map do not decrease.

In other words, rather than solely focusing on binarization, the focus should shift towards improving the coding efficiency of the feature map and reducing the overall bit count of feature map after TSVD transition. This might be a more challenging task compared to pure binarization.

References

- Avriel, M. 2003. *Nonlinear programming: analysis and methods*. Courier Corporation.
- Chen, H.; Wang, Y.; Xu, C.; Shi, B.; Xu, C.; Tian, Q.; and Xu, C. 2020. AdderNet: Do we really need multiplications in deep learning? In *Proceedings of the IEEE/CVF conference on computer vision and pattern recognition*, 1468–1477.
- Courbariaux, M.; Bengio, Y.; and David, J.-P. 2015. Binaryconnect: Training deep neural networks with binary weights during propagations. *Advances in neural information processing systems*, 28.
- Devlin, J.; Chang, M.-W.; Lee, K.; and Toutanova, K. 2018. Bert: Pre-training of deep bidirectional transformers for language understanding. *arXiv preprint arXiv:1810.04805*.
- Dinarelli, M.; and Grobol, L. 2019. Seq2biseq: Bidirectional output-wise recurrent neural networks for sequence modelling. *arXiv preprint arXiv:1904.04733*.
- Frantar, E.; and Alistarh, D. 2023. SparseGPT: Massive Language Models Can Be Accurately Pruned in One-Shot. *ArXiv abs/2301.00774*.
- Frantar, E.; Ashkboos, S.; Hoefler, T.; and Alistarh, D. 2022. GPTQ: Accurate Post-Training Quantization for Generative Pre-trained Transformers. *arXiv preprint arXiv:2210.17323*.
- Guo, K.; Lin, Z.; Xing, X.; Liu, F.; and Xu, X. 2022. Compact Model Training by Low-Rank Projection with Energy Transfer. *arXiv preprint arXiv:2204.05566*.
- He, K.; Zhang, X.; Ren, S.; and Sun, J. 2016. Deep residual learning for image recognition. In *Proceedings of the IEEE conference on computer vision and pattern recognition*, 770–778.
- Jaderberg, M.; Vedaldi, A.; and Zisserman, A. 2014. Speeding up convolutional neural networks with low rank expansions. *arXiv preprint arXiv:1405.3866*.
- Lavin, A.; and Gray, S. 2016. Fast algorithms for convolutional neural networks. In *Proceedings of the IEEE conference on computer vision and pattern recognition*, 4013–4021.
- Li, Y.; Lin, S.; Liu, J.; Ye, Q.; Wang, M.; Chao, F.; Yang, F.; Ma, J.; Tian, Q.; and Ji, R. 2021. Towards compact cnns via collaborative compression. In *Proceedings of the IEEE/CVF Conference on Computer Vision and Pattern Recognition*, 6438–6447.
- Liu, Z.; Lin, Y.; Cao, Y.; Hu, H.; Wei, Y.; Zhang, Z.; Lin, S.; and Guo, B. 2021. Swin transformer: Hierarchical vision transformer using shifted windows. In *Proceedings of the IEEE/CVF international conference on computer vision*, 10012–10022.

Liu, Z.; Mao, H.; Wu, C.-Y.; Feichtenhofer, C.; Darrell, T.; and Xie, S. 2022. A convnet for the 2020s. In *Proceedings of the IEEE/CVF Conference on Computer Vision and Pattern Recognition*, 11976–11986.

Merity, S.; Xiong, C.; Bradbury, J.; and Socher, R. 2016. Pointer Sentinel Mixture Models. *arXiv:1609.07843*.

Mishra, A.; Latorre, J. A.; Pool, J.; Stosic, D.; Stosic, D.; Venkatesh, G.; Yu, C.; and Micikevicius, P. 2021. Accelerating sparse deep neural networks. *arXiv preprint arXiv:2104.08378*.

Neill, J. O. 2020. An overview of neural network compression. *arXiv preprint arXiv:2006.03669*.

Raffel, C.; Shazeer, N.; Roberts, A.; Lee, K.; Narang, S.; Matena, M.; Zhou, Y.; Li, W.; and Liu, P. J. 2019. Exploring the Limits of Transfer Learning with a Unified Text-to-Text Transformer. *arXiv e-prints*.

Russakovsky, O.; Deng, J.; Su, H.; Krause, J.; Satheesh, S.; Ma, S.; Huang, Z.; Karpathy, A.; Khosla, A.; Bernstein, M.; Berg, A. C.; and Fei-Fei, L. 2015. ImageNet Large Scale Visual Recognition Challenge. *International Journal of Computer Vision (IJCV)*, 115(3): 211–252.

Wang, A.; Singh, A.; Michael, J.; Hill, F.; Levy, O.; and Bowman, S. R. 2018. GLUE: A multi-task benchmark and analysis platform for natural language understanding. *arXiv preprint arXiv:1804.07461*.

You, H.; Chen, X.; Zhang, Y.; Li, C.; Li, S.; Liu, Z.; Wang, Z.; and Lin, Y. 2020. Shiftaddnet: A hardware-inspired deep network. *Advances in Neural Information Processing Systems*, 33: 2771–2783.

Zafir, O.; Larey, A.; Boudoukh, G.; Shen, H.; and Wasserblat, M. 2021. Prune once for all: Sparse pre-trained language models. *arXiv preprint arXiv:2111.05754*.

Zhang, S.; Roller, S.; Goyal, N.; Artetxe, M.; Chen, M.; Chen, S.; Dewan, C.; Diab, M.; Li, X.; Lin, X. V.; Mihaylov, T.; Ott, M.; Shleifer, S.; Shuster, K.; Simig, D.; Koura, P. S.; Sridhar, A.; Wang, T.; and Zettlemoyer, L. 2022. OPT: Open Pre-trained Transformer Language Models. *arXiv:2205.01068*.

Zhang, X.; Zou, J.; He, K.; and Sun, J. 2015. Accelerating very deep convolutional networks for classification and detection. *IEEE transactions on pattern analysis and machine intelligence*, 38(10): 1943–1955.

Zhang, Y.; Zhang, Z.; and Lew, L. 2022. Pokebnn: A binary pursuit of lightweight accuracy. In *Proceedings of the IEEE/CVF Conference on Computer Vision and Pattern Recognition*, 12475–12485.

Supplemental Materials

S1 Proof

S1.1 Proof of Eq (3)

Table S1: Computing Cost in TSVD

operator	\times	$+$	compute cost(equivalent +)
$W(\cdot)$	MN	MN	$MN(d-1)$
$U(\cdot)$	-	rMK	rMK
$\text{diag}(s)(\cdot)$	K	-	$K(d-2)$
$V(\cdot)$	-	rKN	rKN
$U \text{diag}(s)V(\cdot)$	K	$rK(M+N)$	$rK(M+N) + (d-2)K$

Proof. The cost of computing each component in TSVD is shown in table S2. Therefore, the critical rank \bar{K} should be such that:

$$r\bar{K}(M+N) + (d-2)\bar{K} = MN(d-1)$$

which is equivalent to eq (3). \square

S1.2 Proof of Eq (4)

We notice an obvious lemma:

Lemma 1. For any $x \in \mathbb{R}^N$, and any ternary vector $x_T \in \{\pm 1, 0\}^N$, we define n as the count of non-zero elements in x_T . We can then construct a ternary vector x'_T such that for any $i \in [0, N)$:

$$x'_T[i] = \begin{cases} \text{sign}(x[i]) & \text{if } \text{abs}(x[i]) \text{ is the top-}n \text{ elements of } \text{abs}(x) \\ 0, & \text{else} \end{cases}$$

It follows that:

$$\begin{aligned} \langle x'_T, x \rangle &\geq \langle x_T, x \rangle \\ \|x'_T\| &= \|x_T\| \end{aligned}$$

Therefore, if the optimal value of x_T^* does not satisfy eq (4), we can utilize lemma 1 to construct a superior x'_T . However, this contradicts the optimality of x_T^* .

S1.3 Proof of Theorem 1

We proof the following lemma:

Lemma 2. Assuming $a \in \mathbb{R}_+^N$, where $a[0] \geq a[1] \geq \dots \geq a[N-1] \geq 0$ and $\|a\| = 1$, it follows that:

$$\min_a \max_{1 \leq k \leq N} \frac{\sum_{i=0}^{k-1} a[i]}{\sqrt{k}} = \gamma_N$$

where γ_N is defined in theorem 1.

remark 3. This lemma is intuitionistic, as it suggests that the minimum value is reached when $\forall k$, $\frac{\sum_{i=0}^{k-1} a[i]}{\sqrt{k}}$ remains constant. However, a rigorous proof is complex and is demonstrated as below. Once lemma 2 is proven, we can easily deduce theorem 1 by incorporating the structure outlined in lemma 1.

Proof. We can divide the feasible region of a into N parts by introducing an additional constraint $C(k')$, $1 \leq k' \leq N$. This constraint is defined as follows:

$$\arg \max_{1 \leq k \leq N} \frac{\sum_{i=0}^{k-1} a[i]}{\sqrt{k}} = k'$$

under such constraint, it follow that:

$$\min_{a, C(k')} \max_{1 \leq k \leq N} \frac{\sum_{i=0}^{k-1} a[i]}{\sqrt{k}} = \min_{a, C(k')} \frac{\sum_{i=0}^{k'-1} a[i]}{\sqrt{k'}} \quad (\text{S1})$$

Now, we can express the optimization problem in equation (S1) with $C(k')$ in a standard form:

$$\begin{cases} \min \frac{1}{\sqrt{k'}} b^\top a \\ \text{s.t.} -Qa \leq 0 & a \text{ is decrease by index} \\ (I-L) \text{diag}(v)^{-1} Q^{-1\top} a \leq 0 & \text{equivalent to } C(k') \\ \|a\|^2 - 1 = 0 \end{cases} \quad (\text{S2})$$

where I is the identity matrix, Q, L, v, b is defined as follow:

$$Q = \begin{pmatrix} 1 & -1 & & & \\ & 1 & -1 & & \\ & & \ddots & \ddots & \\ & & & 1 & -1 \\ & & & & 1 \end{pmatrix}, L = \begin{pmatrix} \dots & 0 & 1 & 0 & \dots \\ \dots & 0 & 1 & 0 & \dots \\ & & & \vdots & \\ \dots & 0 & 1 & 0 & \dots \end{pmatrix}$$

$$v = (1 \quad \sqrt{2} \quad \dots \quad \sqrt{N})^\top, b = (1 \dots 1 \quad 0 \dots 0)^\top$$

L has only one vector with all elements equal to 1 on its k' -th column, b has 1 on its first k' indices. Therefore,

$$Q^{-1\top} = \begin{pmatrix} 1 & & & & \\ 1 & 1 & & & \\ \vdots & \vdots & \ddots & & \\ 1 & 1 & \dots & 1 \end{pmatrix}$$

Now, we will construct a less restrictive problem in comparison to eq (S2)

$$\begin{cases} \min \frac{1}{\sqrt{k'}} b^\top a \\ \text{s.t.} -Qa \leq 0 & a \text{ is decrease by index} \\ (I-L) \text{diag}(v)^{-1} Q^{-1\top} a \leq 0 & \text{equivalent to } C(k') \\ \|a\|^2 - 1 \leq 0 & \text{relax condition 1} \\ 1 - v^\top Qa \leq 0 & \text{relax condition 2} \end{cases} \quad (\text{S3})$$

The reason for the relaxed condition 2 in equation (S3) is that the set $\{a \mid -Qa \leq 0\}$ is a convex cone based on the column vector of Q^{-1} . Additionally, the function f defined as

$$f(a) = \|a\| - v^\top Qa$$

is convex, and for each column vector in Q^{-1} , denoted as a' , it must satisfy $f(a') = 0$. Therefore,

$$f(a) = \|a\| - v^\top Qa \leq 0, \forall a \in \{a \mid -Qa \leq 0\}$$

which is equivalent to relax condition 2 in eq (S3) after normalization of $\|a\| = 1$. Noticing that the feasible area of (S3) is convex, we can apply the Karush-Kuhn-Tucker Conditions (Avriel 2003) to obtain the necessary and sufficient conditions for optimal a^* in eq (S3). Specifically, these conditions require the existence of u and w in \mathbb{R}^N , as well as λ and β in \mathbb{R} , such that:

$$\left\{ \begin{array}{l} \frac{1}{\sqrt{k'}} b - Q^\top u + \\ Q^{-1} \text{diag}(v)^{-1} (I - L^\top) w + 2\lambda a^* - \beta Q^\top v = 0 \\ u, w, \beta, \lambda \geq 0 \\ -Qa^* \leq 0 \\ (I - L) \text{diag}(v)^{-1} Q^{-1\top} a^* \leq 0 \\ \|a^*\|^2 - 1 \leq 0 \quad (\text{S4}) \\ 1 - v^\top Qa^* \leq 0 \\ -u^\top Qa^* = 0 \\ w^\top (I - L) \text{diag}(v)^{-1} Q^{-1\top} a^* = 0 \\ \lambda (\|a^*\|^2 - 1) = 0 \\ \beta (1 - v^\top Qa^*) = 0 \end{array} \right.$$

We can verified that $\|Q^\top v\| = \frac{1}{\gamma_N}$ and the solution presented below is a KKT point.

$$\left\{ \begin{array}{l} u = 0 \\ w = \gamma_N^2 \text{diag}(v) Q Q^\top v \\ a^* = \gamma_N Q^\top v \\ \lambda = \frac{\gamma_N}{2} \\ \beta = 2\gamma_N^2 \\ \text{eq (S3)} = \gamma_N \end{array} \right.$$

Therefore, it is sufficient to be the minimum point of eq (S3), while also being a feasible point of eq (S2). As a result, it can be concluded that it must be the minimum point of eq (S2), which means:

$$\min_{a, C(k')} \frac{\sum_{i=0}^{k'-1} a[i]}{\sqrt{k'}} = \gamma_N$$

Now, if we traverse all possible values of k' , we can obtain:

$$\min_a \max_{1 \leq k \leq N} \frac{\sum_{i=0}^{k-1} a[i]}{\sqrt{k}} = \min_{1 \leq k' \leq N} \min_{a, C(k')} \frac{\sum_{i=0}^{k'-1} a[i]}{\sqrt{k'}} = \gamma_N \quad \square$$

S1.4 Proof of Eq (5)

Proof. We can define a linear mapping H from S to W :

$$H : S \rightarrow W, W = H(S) = U \text{diag}(S) V \quad (\text{S5})$$

Then, it can be easily obtained as follows:

$$H^\top(W) = \text{diag}(U^\top W V^\top)$$

$$H^\top H(S) = [(U^\top U) \odot (V V^\top)](S)$$

Hence, the optimal S^* can be expressed as:

$$S^* = (H^\top H)^\dagger H^\top(W) = [(U^\top U) \odot (V V^\top)]^\dagger \text{diag}(U^\top W V^\top) \quad \square$$

S1.5 Proof of Theorem 2

Proof. We consider the extended SVD decomposition of R_i : $R_i = U \Sigma V$, where U is a unitary matrix with shape $[M, M]$, V is a unitary matrix with shape $[N, N]$, and Σ is a diagonal matrix with shape $[M, N]$. We denote the diagonal vector of Σ as σ_i . We first normalize each column vector in T_u to length 1, denoted as T'_u , and normalize each row vector of T_v to length 1, denoted as T'_v . Note that U and V are fully rank, so we can express T'_u and T'_v on the basis of U and V separately:

$$\begin{aligned} T'_u &= U P_u \\ T'_v &= P_v V \end{aligned}$$

where $P_u = U^\top T'_u, P_v = T'_v V^\top$ are two matrices with shape $[M, 1]$ and $[1, N]$, respectively. From algorithm 1, we can obtain:

$$\begin{aligned} P_u[0, 0] &\geq \cos(\theta) \\ P_v[0, 0] &\geq \cos(\theta) \end{aligned}$$

Therefore,

$$\begin{aligned} \|R_i - T_u \text{diag}(\bar{S}) T_v\|_F^2 &= \min_S \|\mathcal{U} \Sigma \mathcal{V} - \mathcal{U} P_u \text{diag}(S) P_v \mathcal{V}\|_F^2 \\ &= \min_S \|\Sigma - P_u \text{diag}(S) P_v\|_F^2 \end{aligned} \quad (\text{S6})$$

By applying the definition of linear mapping $H : S \rightarrow \Sigma$ in eq (S5), we can expand eq (S6) further as follows:

$$\begin{aligned} &\|R_i - T_u \text{diag}(\bar{S}) T_v\|_F^2 \\ &= \|\Sigma\|_F^2 - \langle H^\top(\Sigma) | (H^\top H)^\dagger | H^\top(\Sigma) \rangle \\ &= \|\Sigma\|_F^2 \\ &- \left\langle \underbrace{\text{diag}(P_u^\top \Sigma P_v^\top)}_{\text{scalar, cause of } q=1} \middle| \underbrace{[(P_u^\top P_u) \odot (P_v P_v^\top)]^\dagger}_{=1} \middle| \underbrace{\text{diag}(P_u^\top \Sigma P_v^\top)}_{\text{scalar, cause of } q=1} \right\rangle \\ &= \|\sigma_i\|_2^2 - \left(\sum_k P_u[k, 0] \sigma_i[k] P_v[0, k] \right)^2 \end{aligned} \quad (\text{S7})$$

Noticing that:

$$\begin{aligned} &\left| \sum_k P_u[k, 0] \sigma_i[k] P_v[0, k] \right| \\ &\geq P_u[0, 0] \sigma_i[0] P_v[0, 0] - \left| \sum_{k \geq 1} P_u[k, 0] \sigma_i[k] P_v[0, k] \right| \\ &\geq \sigma_i[0] \cos^2(\theta) - \underbrace{\sqrt{\sum_{k \geq 1} (P_u[k, 0])^2 \sigma_i[k]^2} \sqrt{\sum_{k \geq 1} (P_v[0, k])^2 \sigma_i[k]^2}}_{\text{Cauchy inequality}} \\ &\geq \sigma_i[0] \cos^2(\theta) - \sigma_i[0] \|P_u[1 : , 0]\|_2 \|P_v[0, 1 :]\|_2 \\ &= \sigma_i[0] \cos^2(\theta) - \sigma_i[0] \sin^2(\theta) = \sigma_i[0] \cos(2\theta) \end{aligned} \quad (\text{S8})$$

Table S2: Cost translation method for computing the difference compression method on a linear mapping $W(\cdot)$ with a d -bit width. The input is a vector, and W is a matrix with shape $[M, N]$. We only consider weight quantization, specifically in the form of $W_{d'}A_d$.

method	hyperparameter	$\times +$ counts	equivalent +	compression rate	acceleration rate
origin	matrix shape $[M, N]$	MN	$(d-1)MN$	1	$\times 1$
SVD	rank K	$MK + KN$	$(d-1)(MK + KN)$	$\frac{MK+KN}{MN}$	$\times \frac{MN}{MK+KN}$
pruning	sparsity r	rMN	$r(d-1)MN$	r	$\times \frac{1}{r}$
quantization	quant form $W_{d'}A_d$	MN	$(d'-1)MN$	$\frac{d'-1}{d-1}$	$\times \frac{d-1}{d'-1}$
		$\times / +$ counts			
TSVD	sparsity r , rank K	$K/rK(M+N)$	$K(d-2) + rK(M+N)$	$\frac{K(d-2)+rK(M+N)}{MN(d-1)}$	$\times \frac{MN(d-1)}{K(d-2)+rK(M+N)}$

Now, by substituting eq (S8) into eq (S7), we can obtain:

$$\begin{aligned}
& \frac{\|R_i - T_u \text{diag}(\bar{S})T_v\|_F^2}{\|R_i\|_F^2} \\
& \leq \frac{\|\sigma_i\|_2^2 - (\sigma_i[0])^2 \cos^2(2\theta)}{\|R_i\|_F^2} \\
& = \frac{\sin^2(2\theta)(\sigma_i[0])^2 + \|\sigma_i[1:] \|_2^2}{\|R_i\|_F^2} \\
& = \frac{\sin^2(2\theta)(\sigma_i[0])^2 + \|\sigma_i[1:] \|_2^2}{(\sigma_i[0])^2 + \|\sigma_i[1:] \|_2^2} \\
& \leq \frac{\sin^2(2\theta)(\sigma_i[0])^2 + (\min(M, N) - 1)(\sigma_i[0])^2}{(\sigma_i[0])^2 + (\min(M, N) - 1)(\sigma_i[0])^2} \\
& = 1 - \frac{\cos^2(2\theta)}{\min(M, N)}
\end{aligned}$$

□

S2 Experiment Detail

S2.1 Experiment Configuration on Figure 1a

In figure 1a, we utilize a self-consistent method to translate the computation costs among quantization, pruning, SVD, and our TSVD, as shown in Table S2. The self-consistency can be verified by observing that the translation of TSVD is precisely equivalent to $W2Ad$ quantization with sparsity consideration. For error, we select relative error of operator norm in figure 1a.

S2.2 Experiment Configuration on Figure 2b

As the unfold matrix \mathcal{W} is sparse, and it is important that the *FLOPS* of $\mathcal{W}(\cdot)$ is only equal to its folding version when considering the sparsity of \mathcal{W} . Therefore, in figure 2b, we have modified translation method of TSVD in table S2 as:

$$\text{compress rate (TSVD)} = \frac{K(d-2) + rK(M+N)}{r'MN(d-1)}$$

where r' is the sparsity rate of \mathcal{W} . The compression rate of Winograd $F(2 \times 2, 3 \times 3)$ is also calculated in this way. All data points in figure 2b are the mean of three runs.

S2.3 Final Network Architecture in Section 4.1

For the sake of brevity, we only present the final architecture of the 7% tolerance TSVD with finetune of ConvNeXt-T model, and have omitted all layer information except for the TSVD layer. The architecture is displayed as below:

```

(convnext): ConvNextModel(
  (embeddings): ConvNextEmbeddings(
    (patch_embeddings): Ternary_SVD_Conv2d(3, 96, kernel_size=(4, 4), stride=(4, 4), form_type=3, rank=63, sparsity=0.269)
  )
  (encoder): ConvNextEncoder(
    (stages): ModuleList(
      (0): ConvNextStage(
        (downsampling_layer): Identity()
        (layers): Sequential(
          (0): ConvNextLayer(
            (dwconv): Ternary_SVD_Conv2d(96, 96, kernel_size=(7, 7), stride=(1, 1), padding=(3, 3), groups=96, form_type=0, rank=5, sparsity=0.235)
            (pwconv1): Ternary_SVD_Linear(in_features=96, out_features=384, bias=True, rank=345, sparsity=0.277)
            (pwconv2): Ternary_SVD_Linear(in_features=384, out_features=96, bias=True, rank=384, sparsity=0.279)
          )
          (1): ConvNextLayer(
            (dwconv): Ternary_SVD_Conv2d(96, 96, kernel_size=(7, 7), stride=(1, 1), padding=(3, 3), groups=96, form_type=0, rank=5, sparsity=0.246)
            (pwconv1): Ternary_SVD_Linear(in_features=96, out_features=384, bias=True, rank=447, sparsity=0.277)
            (pwconv2): Ternary_SVD_Linear(in_features=384, out_features=96, bias=True, rank=414, sparsity=0.277)
          )
          (2): ConvNextLayer(
            (dwconv): Ternary_SVD_Conv2d(96, 96, kernel_size=(7, 7), stride=(1, 1), padding=(3, 3), groups=96, form_type=0, rank=5, sparsity=0.201)
            (pwconv1): Ternary_SVD_Linear(in_features=96, out_features=384, bias=True, rank=435, sparsity=0.278)
            (pwconv2): Ternary_SVD_Linear(in_features=384, out_features=96, bias=True, rank=417, sparsity=0.277)
          )
        )
      )
      (1): ConvNextStage(
        (downsampling_layer): Sequential(
          (1): Ternary_SVD_Conv2d(96, 192, kernel_size=(2, 2), stride=(2, 2), form_type=2, rank=648, sparsity=0.278)
        )
        (layers): Sequential(
          (0): ConvNextLayer(
            (dwconv): Ternary_SVD_Conv2d(192, 192, kernel_size=(7, 7), stride=(1, 1), padding=(3, 3), groups=192, form_type=0, rank=5, sparsity=0.283)
            (pwconv1): Ternary_SVD_Linear(in_features=192, out_features=768, bias=True, rank=763, sparsity=0.276)
            (pwconv2): Ternary_SVD_Linear(in_features=768, out_features=192, bias=True, rank=812, sparsity=0.276)
          )
          (1): ConvNextLayer(
            (dwconv): Ternary_SVD_Conv2d(192, 192, kernel_size=(7, 7), stride=(1, 1), padding=(3, 3), groups=192, form_type=0, rank=5, sparsity=0.246)
            (pwconv1): Ternary_SVD_Linear(in_features=192, out_features=768, bias=True, rank=819, sparsity=0.275)
            (pwconv2): Ternary_SVD_Linear(in_features=768, out_features=192, bias=True, rank=763, sparsity=0.277)
          )
          (2): ConvNextLayer(
            (dwconv): Ternary_SVD_Conv2d(192, 192, kernel_size=(7, 7), stride=(1, 1), padding=(3, 3), groups=192, form_type=0, rank=5, sparsity=0.231)
            (pwconv1): Ternary_SVD_Linear(in_features=192, out_features=768, bias=True, rank=819, sparsity=0.275)
            (pwconv2): Ternary_SVD_Linear(in_features=768, out_features=192, bias=True, rank=882, sparsity=0.275)
          )
        )
      )
      (2): ConvNextStage(
        (downsampling_layer): Sequential(
          (1): Ternary_SVD_Conv2d(192, 384, kernel_size=(2, 2), stride=(2, 2), form_type=2, rank=1152, sparsity=0.273)
        )
        (layers): Sequential(
          (0): ConvNextLayer(
            (dwconv): Ternary_SVD_Conv2d(384, 384, kernel_size=(7, 7), stride=(1, 1), padding=(3, 3), groups=384, form_type=0, rank=5, sparsity=0.280)
            (pwconv1): Ternary_SVD_Linear(in_features=384, out_features=1536, bias=True, rank=1545, sparsity=0.275)
            (pwconv2): Ternary_SVD_Linear(in_features=1536, out_features=384, bias=True, rank=1380, sparsity=0.275)
          )
          (1): ConvNextLayer(
            (dwconv): Ternary_SVD_Conv2d(384, 384, kernel_size=(7, 7), stride=(1, 1), padding=(3, 3), groups=384, form_type=0, rank=5, sparsity=0.231)
            (pwconv1): Ternary_SVD_Linear(in_features=384, out_features=1536, bias=True, rank=1530, sparsity=0.275)
            (pwconv2): Ternary_SVD_Linear(in_features=1536, out_features=384, bias=True, rank=1470, sparsity=0.275)
          )
          (2): ConvNextLayer(
            (dwconv): Ternary_SVD_Conv2d(384, 384, kernel_size=(7, 7), stride=(1, 1), padding=(3, 3), groups=384, form_type=0, rank=5, sparsity=0.231)
            (pwconv1): Ternary_SVD_Linear(in_features=384, out_features=1536, bias=True, rank=1485, sparsity=0.275)
            (pwconv2): Ternary_SVD_Linear(in_features=1536, out_features=384, bias=True, rank=1560, sparsity=0.275)
          )
          (3): ConvNextLayer(
            (dwconv): Ternary_SVD_Conv2d(384, 384, kernel_size=(7, 7), stride=(1, 1), padding=(3, 3), groups=384, form_type=0, rank=5, sparsity=0.241)
            (pwconv1): Ternary_SVD_Linear(in_features=384, out_features=1536, bias=True, rank=1575, sparsity=0.275)
            (pwconv2): Ternary_SVD_Linear(in_features=1536, out_features=384, bias=True, rank=1545, sparsity=0.276)
          )
          (4): ConvNextLayer(
            (dwconv): Ternary_SVD_Conv2d(384, 384, kernel_size=(7, 7), stride=(1, 1), padding=(3, 3), groups=384, form_type=0, rank=5, sparsity=0.256)
            (pwconv1): Ternary_SVD_Linear(in_features=384, out_features=1536, bias=True, rank=1500, sparsity=0.275)
            (pwconv2): Ternary_SVD_Linear(in_features=1536, out_features=384, bias=True, rank=1650, sparsity=0.276)
          )
          (5): ConvNextLayer(
            (dwconv): Ternary_SVD_Conv2d(384, 384, kernel_size=(7, 7), stride=(1, 1), padding=(3, 3), groups=384, form_type=0, rank=5, sparsity=0.280)
          )
        )
      )
    )
  )
)

```

```

        (pwconv1): Ternary_SVD_Linear(in_features=384, out_features=1536, bias=True, rank=1515, sparsity=0.275)
        (pwconv2): Ternary_SVD_Linear(in_features=1536, out_features=384, bias=True, rank=1605, sparsity=0.275)
    )
    (6): ConvNextLayer(
      (dwconv): Ternary_SVD_Conv2d(384, 384, kernel_size=(7, 7), stride=(1, 1), padding=(3, 3), groups=384, form_type=0,
        rank=5, sparsity=0.287)
      (pwconv1): Ternary_SVD_Linear(in_features=384, out_features=1536, bias=True, rank=1440, sparsity=0.275)
      (pwconv2): Ternary_SVD_Linear(in_features=1536, out_features=384, bias=True, rank=1560, sparsity=0.276)
    )
    (7): ConvNextLayer(
      (dwconv): Ternary_SVD_Conv2d(384, 384, kernel_size=(7, 7), stride=(1, 1), padding=(3, 3), groups=384, form_type=0,
        rank=5, sparsity=0.251)
      (pwconv1): Ternary_SVD_Linear(in_features=384, out_features=1536, bias=True, rank=1365, sparsity=0.275)
      (pwconv2): Ternary_SVD_Linear(in_features=1536, out_features=384, bias=True, rank=1590, sparsity=0.276)
    )
    (8): ConvNextLayer(
      (dwconv): Ternary_SVD_Conv2d(384, 384, kernel_size=(7, 7), stride=(1, 1), padding=(3, 3), groups=384, form_type=0,
        rank=5, sparsity=0.252)
      (pwconv1): Ternary_SVD_Linear(in_features=384, out_features=1536, bias=True, rank=1350, sparsity=0.276)
      (pwconv2): Ternary_SVD_Linear(in_features=1536, out_features=384, bias=True, rank=1785, sparsity=0.275)
    )
  )
)
(3): ConvNextStage(
  (downsampling_layer): Sequential(
    (1): Ternary_SVD_Conv2d(384, 768, kernel_size=(2, 2), stride=(2, 2), form_type=2, rank=1975, sparsity=0.275)
  )
  (layers): Sequential(
    (0): ConvNextLayer(
      (dwconv): Ternary_SVD_Conv2d(768, 768, kernel_size=(7, 7), stride=(1, 1), padding=(3, 3), groups=768, form_type=0,
        rank=5, sparsity=0.283)
      (pwconv1): Ternary_SVD_Linear(in_features=768, out_features=3072, bias=True, rank=1740, sparsity=0.275)
      (pwconv2): Ternary_SVD_Linear(in_features=3072, out_features=768, bias=True, rank=3570, sparsity=0.275)
    )
    (1): ConvNextLayer(
      (dwconv): Ternary_SVD_Conv2d(768, 768, kernel_size=(7, 7), stride=(1, 1), padding=(3, 3), groups=768, form_type=0,
        rank=5, sparsity=0.273)
      (pwconv1): Ternary_SVD_Linear(in_features=768, out_features=3072, bias=True, rank=1560, sparsity=0.275)
      (pwconv2): Ternary_SVD_Linear(in_features=3072, out_features=768, bias=True, rank=3390, sparsity=0.275)
    )
    (2): ConvNextLayer(
      (dwconv): Ternary_SVD_Conv2d(768, 768, kernel_size=(7, 7), stride=(1, 1), padding=(3, 3), groups=768, form_type=0,
        rank=5, sparsity=0.281)
      (pwconv1): Ternary_SVD_Linear(in_features=768, out_features=3072, bias=True, rank=1530, sparsity=0.275)
      (pwconv2): Ternary_SVD_Linear(in_features=3072, out_features=768, bias=True, rank=3840, sparsity=0.275)
    )
  )
)
)
)
)
(classifier): Ternary_SVD_Linear(in_features=768, out_features=1000, bias=True, rank=2415, sparsity=0.275)

```